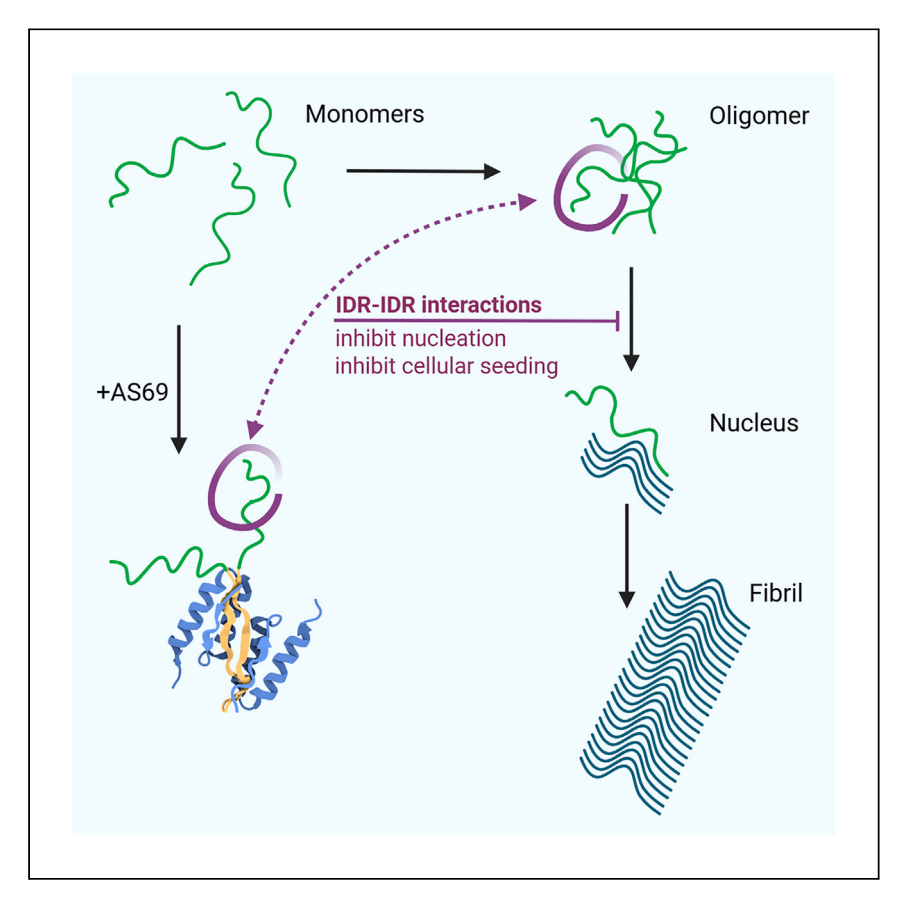


Article

Disordered regions of inhibitor-bound α-synuclein suppress seed-induced fibril nucleation in cells



AS69 is an engineered binding protein that inhibits the aggregation of α -synuclein (α S) involved in Parkinson disease. Schulz et al. report that protein regions remaining intrinsically disordered in the 1:1 complex of α S and AS69 enable interference with the formation of new fibril nuclei.

Celina M. Schulz, Emil D. Agerschou, Luis Gardon, ..., Henrike Heise, Gültekin Tamgüney, Wolfgang Hoyer

wolfgang.hoyer@hhu.de

Highlights

AS69 is a protein-based inhibitor of α -synuclein (α S) fibril nucleation

AS69- α S fusions reveal that the 1:1 AS69: α S complex interacts with α S oligomers

 αS regions remaining intrinsically disordered in the complex support inhibition

Secondary nucleation drives seeding in biosensor cells

Schulz et al., Cell Reports Physical Science 5, 102180

September 18, 2024 © 2024 The Author(s). Published by Elsevier Inc.

https://doi.org/10.1016/j.xcrp.2024.102180





Article

Disordered regions of inhibitor-bound α -synuclein suppress seed-induced fibril nucleation in cells

Celina M. Schulz,¹ Emil D. Agerschou,¹ Luis Gardon,^{1,2} Miriam Alexander,² Matthias Stoldt,^{1,2} Henrike Heise,^{1,2} Gültekin Tamgüney,^{1,2} and Wolfgang Hoyer^{1,2,3,*}

SUMMARY

Inhibitors of amyloid fibril formation can act in diverse ways and aid in elucidating the mechanisms of protein aggregation. The engineered binding protein β-wrapin AS69 binds monomers of Parkinson-disease-associated α -synuclein (α S), yet achieves inhibition at substoichiometric concentration. The substoichiometric activity was not attributed to the binding protein per se, but to its 1:1 complex with α S, in which AS69 sequesters α S residues 30-60 into a globular protein fold, whereas other aS parts remain intrinsically disordered regions (IDRs). Here, we investigate AS69-αS fusion constructs that form the AS69:aS complex by intramolecular folding and expose different IDRs. We find that not only the globular part of the complex but also α S IDRs are critical for substoichiometric inhibition, which is achieved by interference with primary and secondary fibril nucleation. The effects in vitro are reproduced in cellular seeding assays, indicating that secondary nucleation drives seeding in aggregate biosensing.

INTRODUCTION

The formation of amyloid fibrils of the protein α -synuclein (α S) is involved in Parkinson disease, Lewy body dementia, multiple system atrophy, and other synucleinopathies. Amyloid formation is a multistep reaction that in its initial stages passes through a highly unfavorable nucleus state, followed by the energetically favorable addition of monomers to the fibril ends during fibril elongation. In particular, the nucleation of amyloid fibrils is difficult to study, owing to its complexity, the short lifetimes of the nuclei, the inherent heterogeneity that is reflected in the polymorphism of the reaction products, and its poor separability from the subsequent reaction steps. Nevertheless, factors that strongly promote amyloid fibril nucleation could be identified that are thought to contribute to amyloid formation and propagation *in vivo*. For example, lipid membranes of specific composition can enhance α S fibril nucleation, depending on the lipid composition and α S concentration at the membrane surface. Pruthermore, preexisting fibrils can catalyze the formation of new fibril nuclei in a process that is termed secondary nucleation to distinguish it from the primary nucleation, which does not involve preexisting fibrils.

Molecules with the capacity to modulate amyloid formation are of great interest as they help to define the mechanism of protein aggregation and inform the development of therapeutic agents. 12 We recently showed that the β -wrapin AS69, an engineered protein binding the αS monomer, acts as a highly potent inhibitor of primary and secondary nucleation and elongation of αS . 13 AS69 is a dimer of two identical subunits covalently linked by a disulfide bond between the Cys-28 residues of

¹Institut für Physikalische Biologie, Faculty of Mathematics and Natural Sciences, Heinrich Heine University Düsseldorf, 40204 Düsseldorf, Germany

²Institute of Biological Information Processing (IBI-7: Structural Biochemistry), Forschungszentrum Jülich, 52428 Jülich, Germany

³Lead contact

*Correspondence: wolfgang.hoyer@hhu.de https://doi.org/10.1016/j.xcrp.2024.102180





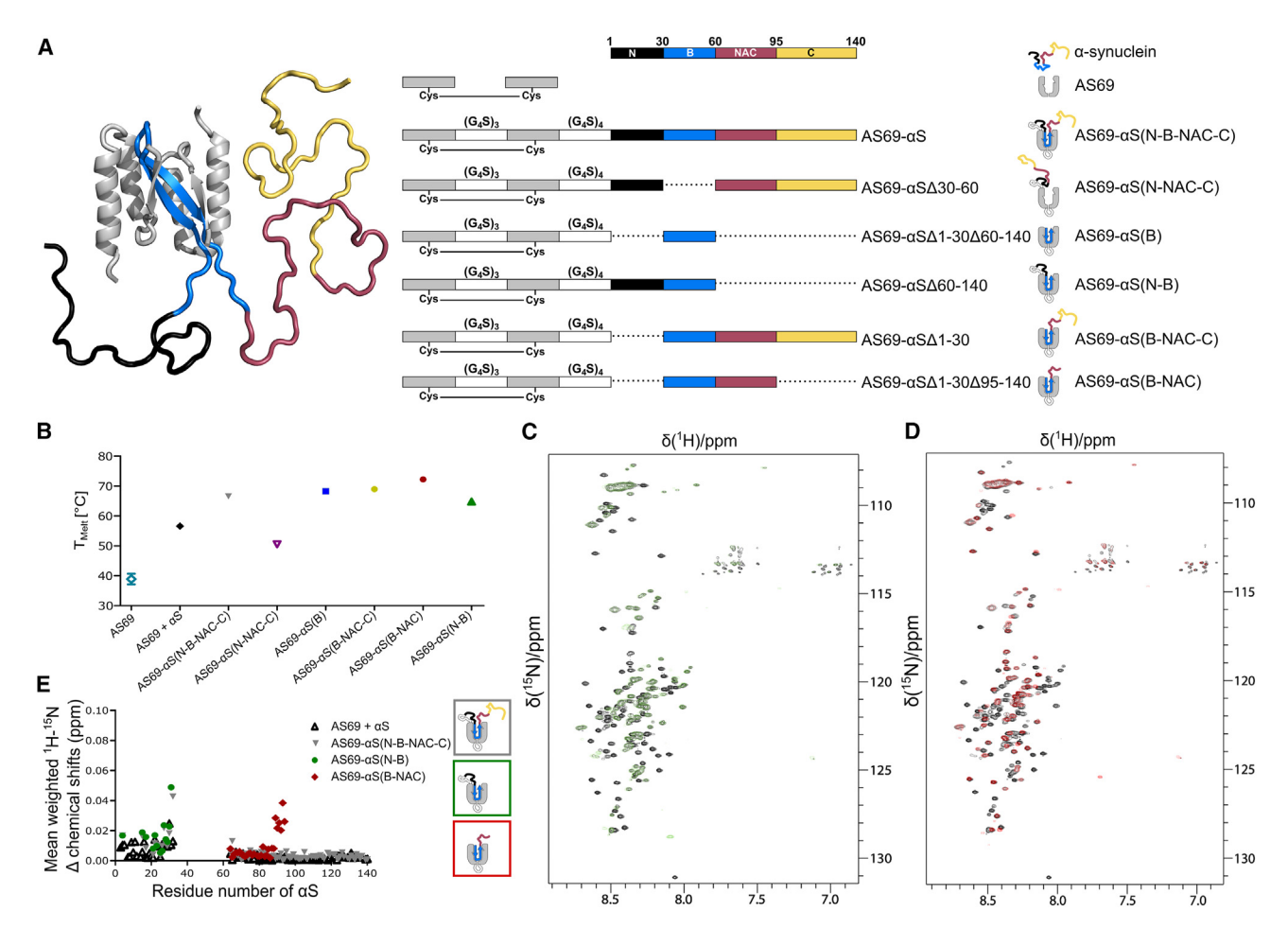


Figure 1. AS69- α S fusion constructs to study the role of α S IDRs in the inhibition of amyloid formation

(A) Structural model of the AS69: α S complex based on NMR (PDB: 4BXL). AS69 (gray) is a homodimer linked through a disulfide bridge. α S locally adopts β -hairpin conformation in the AS69-binding region ("B", blue), while the other α S regions (N terminus, black; NAC region, red; C terminus, yellow) remain intrinsically disordered. Scheme of the primary structure of α S, AS69, and the six AS69- α S fusion constructs investigated; schematic illustration of the conformations of the polypeptide segments in the different constructs and the constructs' nomenclature.

(B) Melting temperatures of free AS69, the intermolecular AS69: α S complex, and the AS69- α S fusion constructs determined by CD spectroscopy at 222 nm, pH 5.0. Melting curves are shown in Figure S2.

 $(C \text{ and D})^{1}H^{-15}N \text{ HSQC NMR spectra of AS69-}\alpha S(N-B) (green, C) \text{ and AS69-}\alpha S(B-NAC) (red, D) overlaid with the one of full-length AS69-}\alpha S(N-B-NAC-C) (black). The spectra were recorded at 10°C, where only the IDR segments but not the complex core are visible.$

(E) Mean weighted $^1H^{-15}N$ chemical shift changes of αS backbone amides in the intermolecular AS69: αS complex and within AS69- αS fusion constructs compared to the chemical shifts of free αS .

both subunits. For inhibition, AS69 induces local folding of the αS region containing residues 37–54 into a β -hairpin conformation in the otherwise intrinsically disordered protein ¹⁴ (Figure 1A). Binding of this αS region can thus inhibit αS aggregation, which has been confirmed by other agents targeting the same αS region, including chaperones. ^{15–17} For AS69, inhibition of fibril elongation could be explained by sequestration of αS monomers, which lose the competence to elongate fibrils when incorporated in the AS69 complex. ¹³ While this inhibitory activity required stoichiometric amounts of AS69, substoichiometric amounts sufficed for the inhibition of primary and secondary nucleation, which is remarkable for a monomer binding agent. ¹³ A fusion construct of AS69 and αS , in which the αS -binding site of AS69 is occupied by the fused αS , showed an inhibition potency on secondary nucleation similar to that of AS69 alone. This indicated that the complex between AS69 and αS is the inhibitory species in secondary nucleation. ¹³ Here, we determined the αS

Article



regions within the AS69: α S complex that assist in substoichiometric inhibition, with the aim to (1) better understand how a monomer binder accomplishes inhibition of amyloid fibril nucleation and to (2) gain further insights into the elusive primary and secondary nucleation mechanisms. We generated a set of AS69- α S fusion constructs that form the AS69: α S complex by intramolecular folding and expose different intrinsically disordered regions (IDRs) of α S. Testing the effects of the fusion constructs on lipid-induced primary nucleation, secondary nucleation, and fibril elongation in vitro, and on seed-induced fibril formation in cells, allowed us to (1) delineate the α S IDRs involved in the inhibition of the different reaction steps, and (2) identify the critical contribution of nucleation processes to aggregate biosensing.

RESULTS

Fusion constructs exhibit intramolecular formation of the AS69:αS complex

We generated a set of six AS69- α S fusion constructs in which two AS69 subunits were fused to one full-length or truncated α S unit (Figures 1A and S1, see also supplemental experimental procedures). The three polypeptide (sub)units were separated by glycine-serine linkers to ensure sufficient conformational flexibility for intramolecular formation of the AS69: α S complex. The construct containing the full-length α S sequence is called here either AS69- α S or AS69- α S(N-B-NAC-C), as it contains all α S segments, the N terminus (residues 1–30), the AS69-binding region (residues 30–60), the NAC region (residues 60–95), and the C terminus (residues 95–140). The other five constructs lack one or more of these α S segments and are named according to the segments they contain (Figure 1A).

Circular dichroism (CD) and NMR spectroscopy were performed to test whether the fusion constructs form the AS69: α S complex. In CD spectroscopy, addition of α S to AS69 results in increased thermostability of AS69 due to coupled folding-binding (Figures 1B and S2). ^{13,18} The melting temperature of the AS69- α S fusion is another 10°C–15°C higher than that of the mixture of AS69 and α S, indicating that intramolecular complex formation within the fusion construct is facilitated compared to intermolecular complex formation. ¹³ Almost all fusion constructs with truncations in the α S segment have thermostabilities similar to that of full-length AS69- α S, with melting temperatures in the range of 65°C–72°C (Figures 1B and S2). The one exception is AS69- α S(N-NAC-C), with a melting temperature of 51°C. This construct lacks the AS69-binding region of α S and is therefore unable to form the AS69: α S complex. The CD data demonstrate that the intramolecular AS69: α S complex is established in all fusion constructs that contain the AS69-binding region of α S.

In $^1\text{H}^{-15}\text{N}$ heteronuclear single quantum coherence (HSQC) NMR spectroscopy performed at 10°C , the globular core of the AS69: α S complex is invisible due to intermediate exchange, leaving only IDRs of α S visible. ¹⁴ This observation is recovered for the fusion constructs (Figures 1C, 1D, S3, and S4). The N, NAC, and C segments of the α S units within the fusion constructs did not show any significant shift changes compared to free α S (Figures 1C–1E, S3, and S4), indicating that intramolecular complex formation does not have a great impact on the flexible conformation of the α S segments that remain intrinsically disordered. By increasing the temperature to 30°C , the globular core of the AS69: α S complex becomes visible in $^1\text{H}^{-15}\text{N}$ HSQC NMR spectroscopy as a set of well-dispersed resonances. ¹⁴ The resonances of the intermolecular AS69: α S complex are reproduced by all fusion constructs that contain the AS69-binding region of α S (Figure S3B). Collectively, the CD and NMR data demonstrate that these fusion constructs form the globular core of the AS69: α S



complex in an intramolecular fashion and present the N, NAC, and/or C segments of αS as IDRs attached to this core. The conformations of the segments in the different constructs are schematically illustrated in Figure 1A.

Validation of the secondary nucleation assay

We tested the effects of the fusion constructs on three individual steps of the aggregation reaction: lipid-induced primary nucleation, secondary nucleation, and fibril elongation. To investigate the primary nucleation of αS , an assay employing 1,2-dimyristoyl-sn-glycero-3-phosphoserine (DMPS) small unilamellar vesicles (SUVs) as a nucleation trigger has been established as a model of lipid-induced αS aggregation, which might represent the main source of primary αS fibril nuclei $in\ vivo.^9$ For fibril elongation, highly seeded assays were performed at neutral pH, resulting in fibrils with lengths in the micrometer range. ¹⁹

With regard to secondary nucleation, in vitro studies have shown that this process is dominant in aS aggregation at slightly acidic pH values and under low-seeded conditions, resulting in rather short fibrils. 19,20 However, limited reproducibility of secondary nucleation assays can pose a challenge. To avoid fragmentation and primary nucleation, the acidic pH should be coupled to guiescent conditions and low concentrations of pre-formed fibrils.^{21,22} We recently devised a secondary nucleation protocol to study how AS69 inhibits secondary nucleation of α S. ¹³ This method produced very consistent kinetic traces within a single seed preparation, and it consistently resulted in the characteristic steep and asymmetric sigmoidal growth curve as measured by in situ fluorescence of the amyloid specific dye thioflavin T (ThT). 23,24 Furthermore, we observed the same characteristic inhibition effects using different seed preparations. 13 However, this required normalization as the absolute rates varied considerably between different seed preparations. Normalization was achieved by dividing the maximal observed growth rate of a sample, r_{max}, by the maximal observed growth rate of uninhibited controls, r_{max,0}, which were run alongside the samples. In the present study, we wanted to further improve the assay to yield more consistent absolute rates. As we observed previously, the secondary nucleation kinetics data were very variable when different seed preparations (prepared under the same conditions) were used (Figure S5). We therefore prepared several seed samples in parallel (from the same initial solution of monomers) and tested them in a pre-run of the secondary nucleation assay (Figure S5). For the final secondary nucleation assays, seed preparations showing homogeneous sigmoidal shapes in the pre-runs were chosen. This yielded increased reproducibility of absolute rates in the secondary nucleation kinetics data (Figure S5).

To validate that the assay is indeed reporting on secondary nucleation, an experiment with varying monomer concentrations was performed (Figure 2). At monomer concentrations below 50 μ M, no exponential increase in fluorescence was observed, indicating no secondary nucleation-triggered formation of amyloid fibrils, probably due to the limited amount of monomers to form precursors on the fibril surface during secondary nucleation. At the same time, an excess of monomers, above about 80 μ M, did not increase the aggregation rate, suggesting that at this concentration, the fibril surface of the added 0.3 μ M fibril seeds (concentration in monomer units) is saturated. Only in the monomer concentration range from 50 to 80 μ M was a pronounced monomer-dependent sigmoidal curve detected. These data are in strong agreement with theoretical simulations of the process. 11 For the subsequent secondary nucleation assays, concentrations of 0.3 μ M fibril seeds and 70 μ M monomer were applied.

Cell Reports Physical Science Article



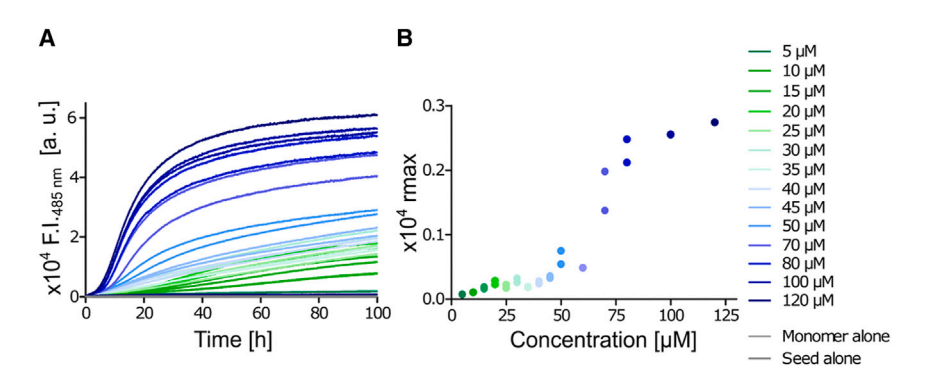


Figure 2. Validation of secondary nucleation assay at pH 5.0 (A) Detection of the change in ThT fluorescence when different concentrations of monomeric α S were incubated in the presence of 0.3 μ M pre-formed fibrils under quiescent conditions. (B) Relative rates of secondary nucleation (r_{max}) plotted against monomer concentration.

The complex of AS69 and α S inhibits fibril nucleation at substoichiometric concentration by interacting with α S oligomers

The inhibitory potential of AS69- α S on elongation, lipid-induced primary nucleation, and secondary nucleation was compared to that of AS69 (Figure 3). For the inhibition of fibril elongation, stoichiometric amounts of AS69 were required, as previously reported (Figure 3A). This can be explained by the sequestration of α S, which cannot be incorporated into the fibril end when bound to AS69. In contrast, AS69- α S does not inhibit fibril elongation, in line with preoccupation of the AS69 binding site with the fused α S (Figure 3A). This interpretation is supported by the restoration of inhibition only for the one fusion construct that lacks the part of α S that binds to AS69 (AS69- α S(N-NAC-C)), which renders the AS69 part of this construct capable of sequestering free α S as confirmed by the thermostability measurements (Figures S6–S8).

In DMPS SUV-induced primary nucleation at pH 6.5, α S fibril nuclei are formed on the lipid surface and grow exclusively by elongation into long fibrils (Figure 3B). To reduce the rate of lipid-induced primary nucleation to 50% (i.e., $r_{max}/r_{max,0} = 0.5$), a 1:10 ratio of inhibitor to α S monomer was required for both AS69 and AS69- α S (Figure 3B). α S fibril amplification by secondary nucleation at low pH results in short fibrils (Figure 3C). As for primary nucleation, AS69 and AS69- α S showed similar effects, in this case with a 1:50 ratio of inhibitor to α S monomer required for 50% inhibition (Figure 3C). The activity of AS69- α S, with its pre-occupied α S binding site in the AS69 part, in the primary and secondary nucleation assays indicates that the free binding site of AS69 is not involved in the inhibition of nucleation processes. Instead, it is the 1:1 complex of AS69 and α S that exerts the inhibitory activity.

The substoichiometric activity requires an interaction of AS69- α S with higher-order α S assemblies. For example, AS69- α S might bind to pre-nucleus oligomers and prohibit their conversion to amyloid fibrils. We applied sucrose density gradient centrifugation (DGC) to analyze the size distribution of α S species at the end of aggregation assays in the absence and presence of AS69- α S (Figure 4A). DGC allows the separation of α S monomers, oligomers, and larger species such as fibrils or condensates (Figure 4B). The end of the secondary nucleation assay in the absence of AS69- α S, the majority of α S was found in the lower DGC fractions 12–14, reflecting the formation of amyloid fibrils (Figure 4D). In addition, monomers were still detectable in fractions 1–4, but no oligomeric species between fractions 4 and 12. When the secondary nucleation assay was carried out in the presence of increasing concentrations



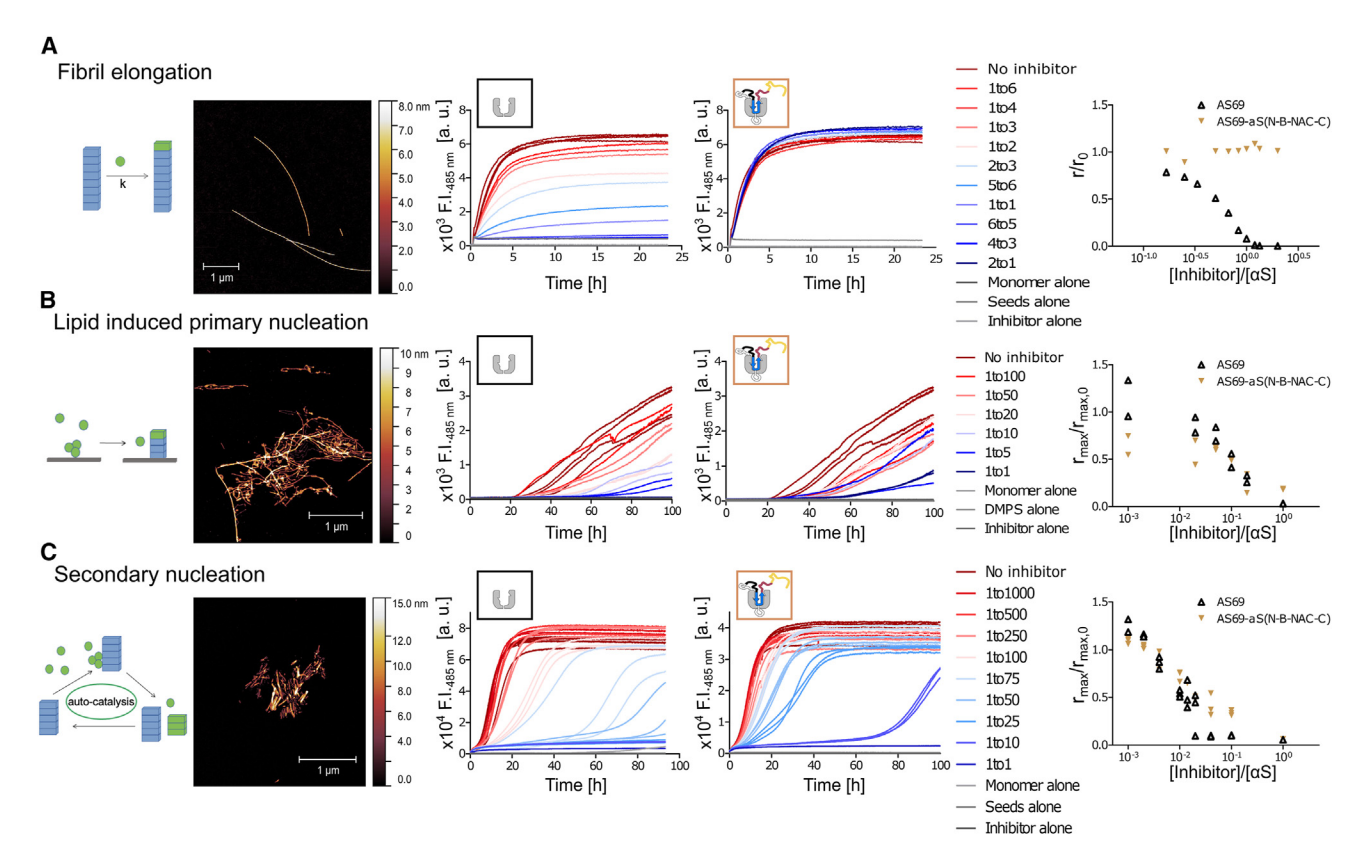


Figure 3. Fusion of α S to AS69 has different consequences for inhibition of fibril elongation, lipid-induced primary nucleation, and secondary nucleation

From left to right: Schematic of the individual reaction step investigated; AFM of fibrils generated in the different aggregation assays; ThT fluorescence time traces of the aggregation assays in the presence of different concentrations of AS69 (left) or AS69- α S(N-B-NAC-C) (right), including indicated controls; relative aggregation rates compared to uninhibited control. Conditions: (A) fibril elongation, 25 μ M monomeric α S was incubated in the presence of 2.5 μ M pre-formed fibrils under quiescent conditions, pH 7.4; (B) lipid-induced primary nucleation, 70 μ M monomeric α S was incubated in the presence of 70 μ M DMPS SUV under quiescent conditions, pH 6.5; (C) secondary nucleation, 70 μ M monomeric α S was incubated in the presence of 0.3 μ M pre-formed fibrils under quiescent conditions, pH 5.0. The different inhibitor-to-monomer ratios used in each assay are shown in a color gradient from red to blue. Negative controls are shown in gray shades and the positive control (No inhibitor) in dark red.

of AS69- α S, the formation of large aggregates localizing to the low DGC fractions was essentially abrogated (Figures 4E–4G), in agreement with the low ThT fluorescence intensity (Figure 4A). Instead, increasing α S amounts were found in the intermediate fractions 5–8, reflecting the population of oligomeric states. According to the band intensity in SDS-PAGE, the amount of α S within these oligomers was much lower than the amount of α S monomers (Figures 4E–4G) and also much smaller than the amount of fibrillar α S in the assay performed in the absence of AS69- α S (Figure 4D). AS69- α S colocalized with α S in the oligomer fractions 5–8. These findings suggest that AS69- α S inhibits fibril nucleation by interacting with α S oligomers, which leads to the stabilization of low amounts of oligomers. The SDS band intensities for the sample at a 1:5 inhibitor:substrate ratio allowed to compare the partitioning of α S and AS69- α S into monomer and oligomer states (Figure 4G). α S and AS69- α S exhibited similar monomer:oligomer distributions, indicating similar propensities to integrate into oligomers.

α S IDRs of AS69- α S are required for nucleation inhibition

To gain further insight into how the 1:1 complex of AS69 and α S inhibits nucleation processes, we next tested the inhibitory potential of the set of AS69- α S fusion



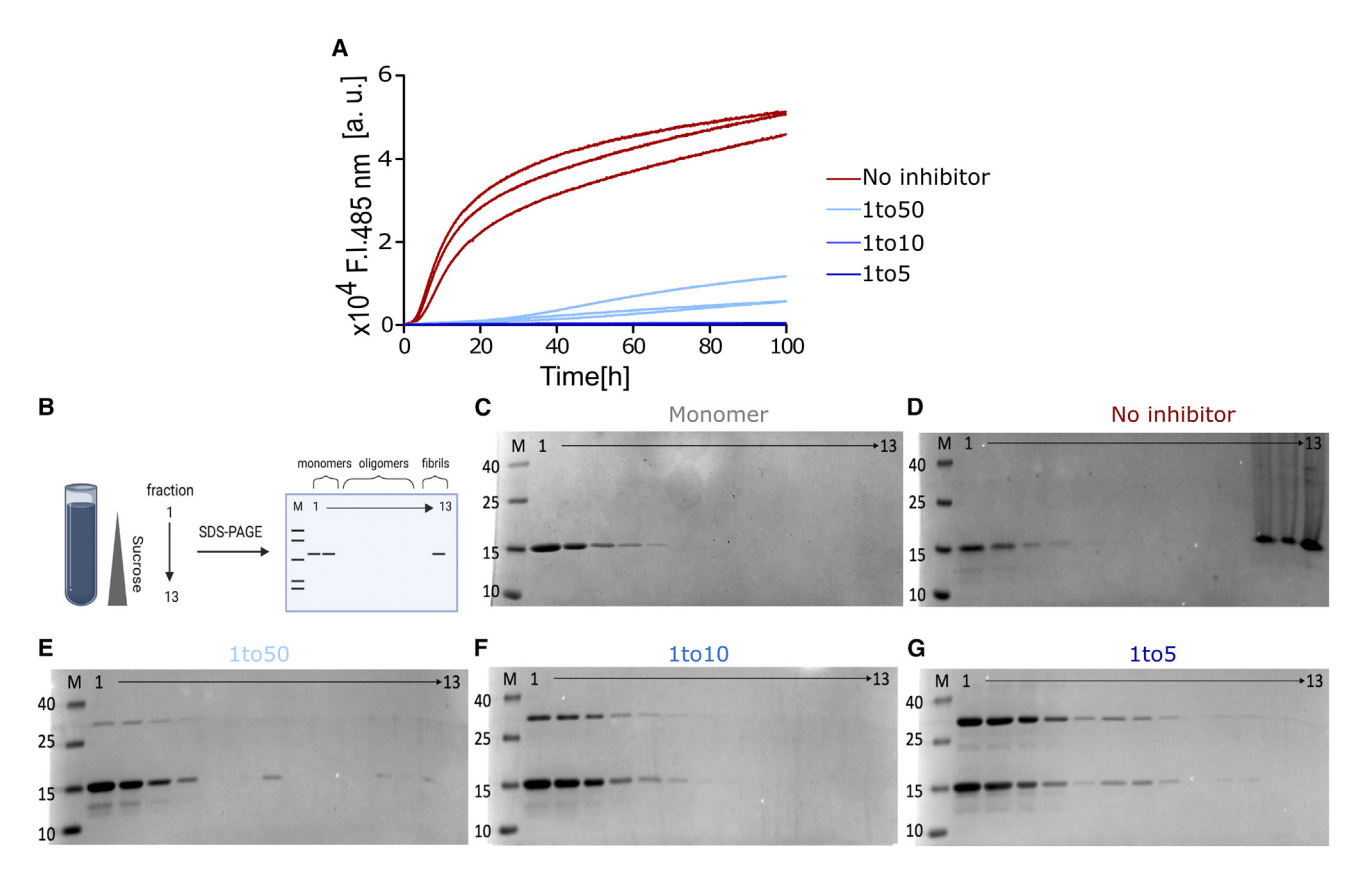


Figure 4. AS69- α S inhibits fibril nucleation by interacting with α S oligomers

(A) ThT fluorescence time traces of secondary nucleation assays in the presence of different concentrations of AS69- α S(N-B-NAC-C). (B) Schematic of the DGC assay.

(C-G) Tris/Tricine SDS-PAGE gels show the distributions of αS and AS69- αS (N-B-NAC-C) within the DGC gradients from left to right corresponding to the fractions from top to bottom of each gradient. Monomeric proteins are found in the top (left) fractions, oligomers in the center fractions, and fibrils in the bottom (right) fractions.

constructs on lipid-induced primary nucleation and secondary nucleation. In the fusion constructs, the AS69: α S complex is pre-formed (with the exception of AS69- α S(N-NAC-C) lacking the binding region), and different (or no) IDRs of α S are exposed on the exterior of the globular part of the complex.

The construct AS69- α S(B), in which all α S IDRs are deleted, does not exhibit substoichiometric inhibition of nucleation. This demonstrates that α S IDRs, although not directly taking part in binding to AS69, are involved in substoichiometric inhibition of nucleation processes (Figures 5A, S9, and S10). The fusion construct where the N-terminus of α S had been removed (AS69- α S(B-NAC-C)) was inhibiting both lipid-induced primary nucleation and secondary nucleation as strongly as AS69 (Figures 5B, S9, and S10), showing that the N-terminal IDR is not required for the inhibition of nucleation. Additional truncation of the C terminus (AS69- α S(B-NAC)) also did not reduce the inhibitory activity (Figure 5B). Thus, the presence of the NAC IDR exposed on the globular part of the AS69: α S complex is sufficient for substoichiometric inhibition of fibril nucleation. Interestingly, the construct AS69- α S(N-B), lacking the NAC IDR, showed substoichiometric inhibition of secondary nucleation but not lipid-induced primary nucleation (Figure 5C). This demonstrates that the two nucleation processes have different susceptibilities with the regard to the presence of α S IDRs. For inhibition of secondary nucleation, the presence of



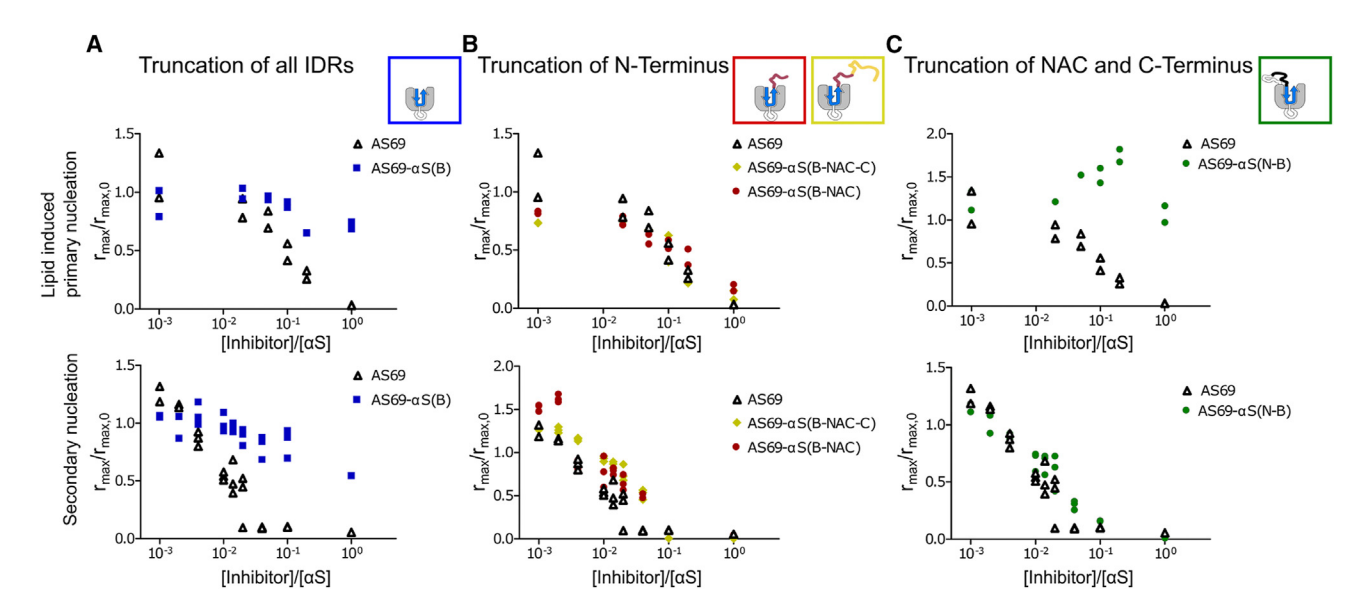


Figure 5. Truncated versions of the AS69-αS fusion inhibit primary and secondary nucleation
Relative rates of lipid-induced primary nucleation (top row) and secondary nucleation (bottom row) with increasing concentration of truncated versions of AS69-αS(N-B-NAC-C) fusion constructs (inhibitor) in dependence on the inhibitor-to-monomer ratios. Data are shown for truncation of all IDRs (A), of N-terminal IDR (B), and of NAC and C-terminal IDRs (C). The time traces used to derive the relative rates are shown in Figures S9 and S10.

either the NAC IDR or the N-terminal IDR is sufficient. In contrast, inhibition of lipid-induced primary nucleation strictly requires the presence of the NAC IDR.

α S IDRs act in concert with the globular AS69: α S domain

It is noteworthy that inhibition requires the parts of αS that are not interacting with AS69 to accomplish inhibition of primary and secondary nucleation. It was therefore of interest to investigate whether these IDRs could have inhibitory effects on their own without AS69 altogether. For this reason, we investigated whether αS fragments would be able to accomplish inhibition of primary and secondary nucleation on their own or when fused to the linker employed in the fusion constructs. The fragments (1) N terminus without AS69 binding site (α S(1-37), or in domain notation αS(N-B_{aa31-37})) (aa, amino acids) and (2) N terminus without AS69 binding site containing (G₄S)₄-linker ((G₄S)₄- α S(N-B_{aa31-37})), (3) α S(NAC-C), and (4) α S(N-NAC-C) were investigated as peptides without fusion to AS69 (Figure 6A). Hardly any inhibition of primary or secondary nucleation was observed for the N-terminal peptides with and without the linker (Figures 6, S11, and S12). Hence, the N-terminal IDR on its own is not sufficient to accomplish inhibition but needs to be in complex with AS69 for inhibitory activity. For the fragments including the NAC and C regions, no inhibition of primary nucleation but some inhibition of secondary nucleation was observed (Figure 6). Inhibition of secondary nucleation occurred at stoichiometric inhibitor concentrations and was therefore weaker than that of the corresponding AS69 fusions. In conclusion, the substoichiometric inhibition of the AS69-αS fusions was not observed for the corresponding isolated αS IDR fragments, which shows that αS IDRs act in concert with the globular part of the AS69: αS complex in the inhibition of fibril nucleation.

The constructs' potency to inhibit seed-induced aggregation in cells correlates with their potency to inhibit fibril nucleation

The transmission of protein aggregates to cells that express fluorescent monomeric proteins is a method to determine the seeding activity of aggregates. The



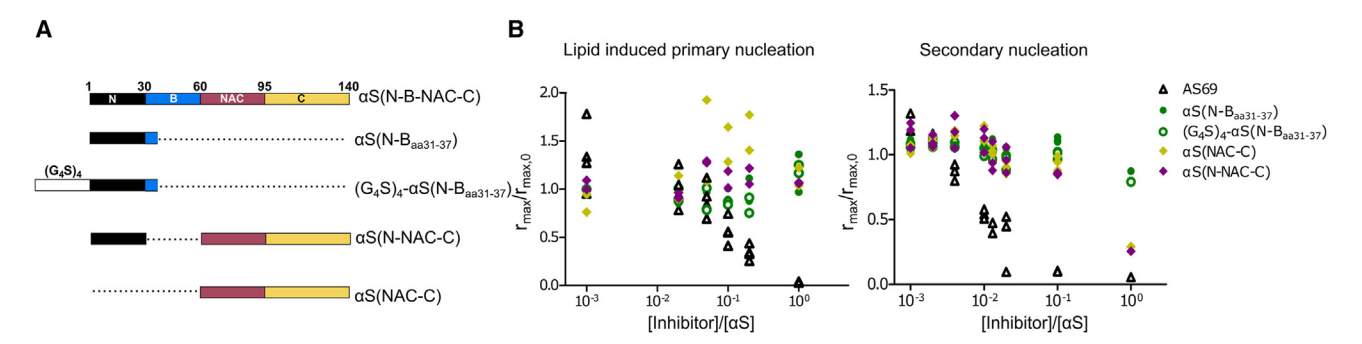


Figure 6. Effects of truncated versions of αS on the nucleation of full-length αS

(A) Schematic overview of the sequence of αS and the four truncated versions investigated.

(B) Relative aggregation rates of lipid-induced primary nucleation and secondary nucleation with increasing concentrations of truncated versions of αS monomers (inhibitor) are plotted against the inhibitor-to-monomer ratios. The time traces used to derive the relative rates are shown in Figures S11 and S12.

emergence of fluorescent puncta indicates that aggregates converted the monomeric substrates to an aggregated state. Such biosensor cell assays can, for example, be applied to test the ability of compounds to interfere with aggregate spreading. Here, we tested the ability of the AS69- α S fusion constructs to interfere with seeding in HEK cells expressing yellow fluorescent protein (YFP)-labeled α S containing the A53T mutation (Figure 7A). α SA53T occurs in familial Parkinson disease and is more aggregation prone than wild-type α S.

When αS fibril seeds prepared *in vitro* were added to the cells, >50% of the cells showed the emergence of fluorescent puncta over the course of 3 days, which were absent when no seeds were added (Figures 7B–7D, positive vs. negative control). Addition of AS69- αS (N-B-NAC-C) strongly inhibited seeded aggregation (Figures 7B and 7E), in line with its effects on fibril nucleation *in vitro*. AS69- αS (B-NAC-C), AS69- αS (B-NAC), and AS69- αS (N-B), the three other constructs that inhibited secondary nucleation *in vitro*, were also effective at the inhibition of cellular seeding (Figures 7B and 7G–7I). In contrast, AS69- αS (B), which did not inhibit fibril nucleation *in vitro*, also did not inhibit cellular seeding (Figures 7B and 7F). The correlation of the inhibitory effects on nucleation *in vitro* and on cellular seeding suggest that aggregate proliferation in biosensor cells is not just a consequence of fibril seed elongation but also involves secondary nucleation of amyloid fibrils on the surface of the added seeds.

As recombinant proteins are transfected into cells, AS69- α S and its variants are expected to be degraded relatively quickly. However, they inhibit seeded aggregation over the course of 3 days. We did not analyze the time-dependent concentrations of intact proteins. Due to the substoichiometric activity, low concentrations of the inhibitors may suffice to inhibit seeded aggregation. Furthermore, in the cell assay, compounds were co-transfected with fibril seeds and might have been stabilized by attaching to the seeds, possibly at the critical sites of secondary nucleation, already before entering the cellular milieu.

DISCUSSION

Due to the complexity of protein aggregation mechanisms, inhibitors can act in various ways. 26,27 β -Wrapin AS69 is an engineered binding protein that sequesters the αS region containing as 30–60 by inducing a local β -hairpin conformation while the other regions of αS remain intrinsically disordered. 14 The mechanisms of inhibition of αS aggregation and the involved αS regions identified in this work are



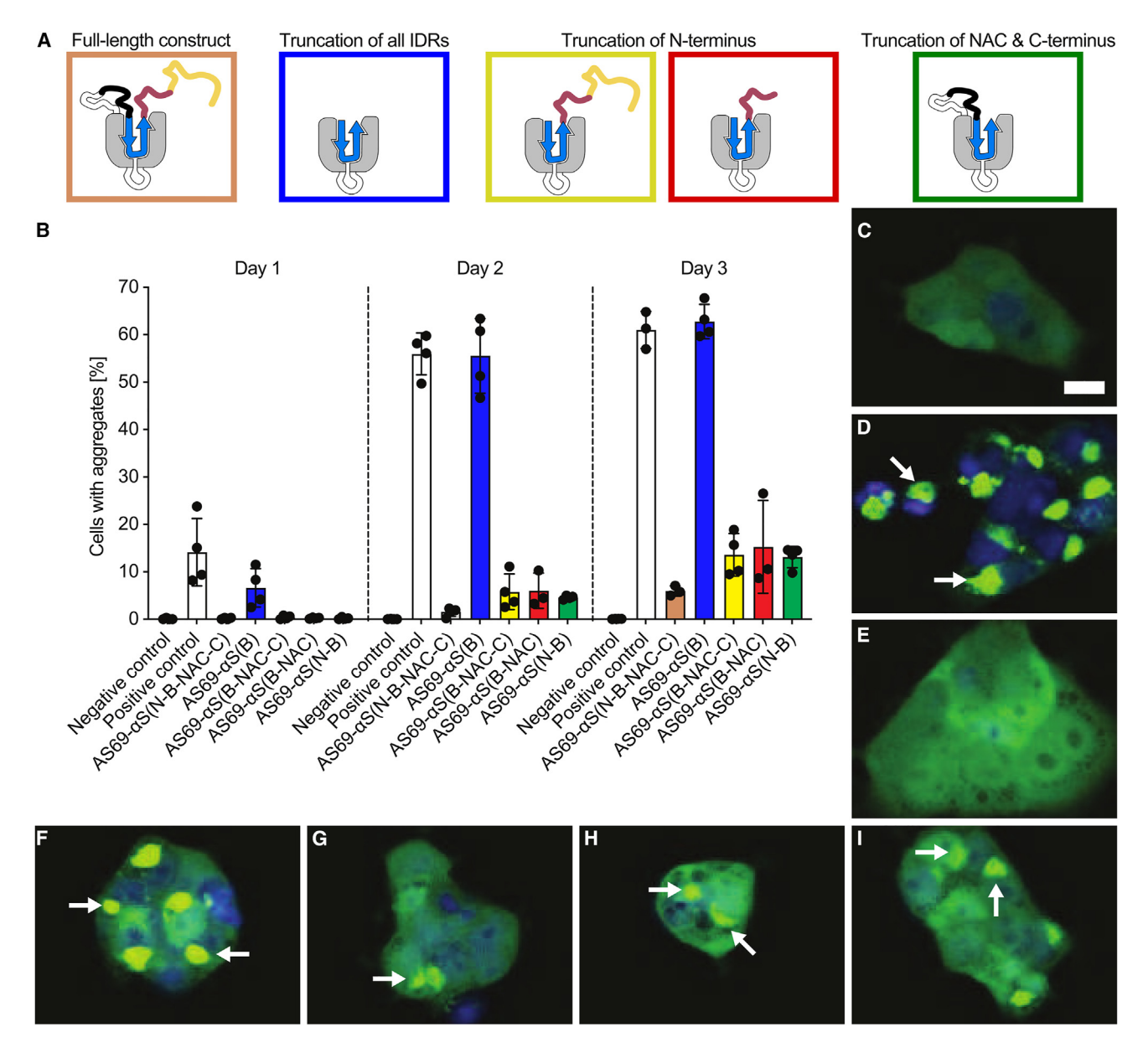


Figure 7. N- or C-terminal IDRs of α S confer AS69-mediated inhibition of seeding in biosensor cells

(A) Overview of full-length and truncated AS69- α S constructs tested in regard to their ability to inhibit seeded aggregation of α S in α SA53T-YFP cells, which are HEK293T cells that stably express human α S with the familial A53T mutation fused to YFP. The cells allow fluorescence-based detection of α S aggregates, which appear as highly fluorescent intracellular puncta after seeding.

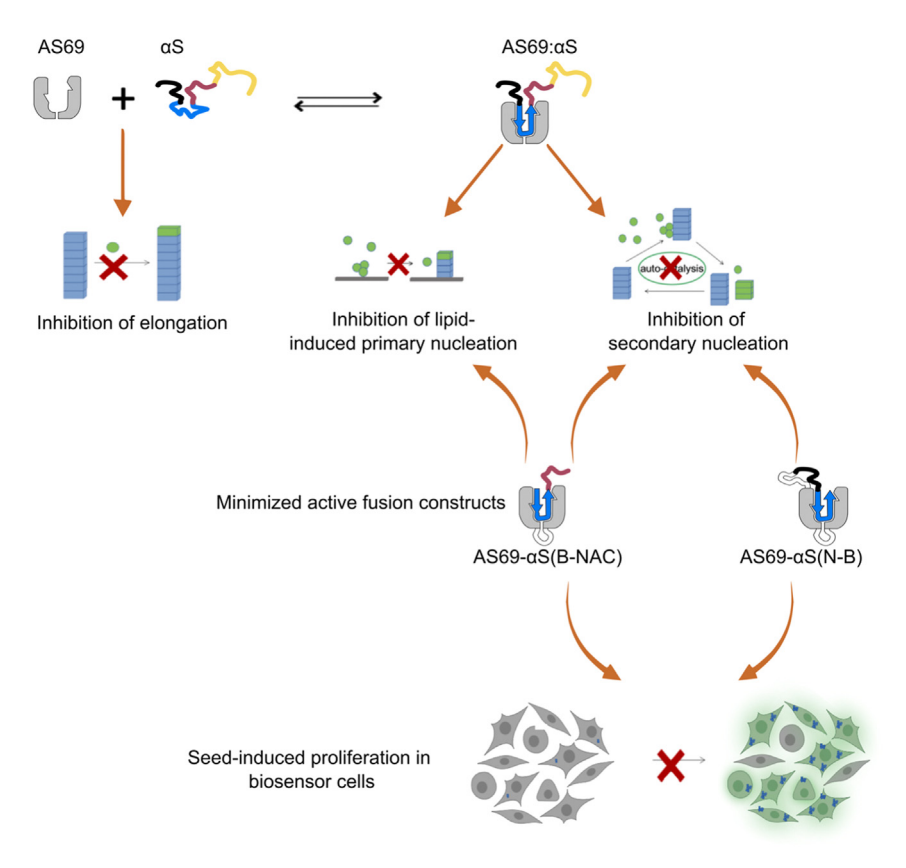
(B) Fraction of cells containing aggregates without seeding (negative control), with seeding with αS fibrils in the absence of inhibitors (positive control), or with seeding with αS fibrils in the presence of the indicated AS69- αS constructs. Data are represented as mean \pm SEM.

(C–I) Fluorescence microscopy images of cells after day 3 under the following conditions: (C) negative control, (D) positive control, (E) with AS69- α S(N-B-NAC-C), (F) with AS69- α S(B), (G) with AS69- α S(B-NAC-C), (H) with AS69- α S(B-NAC), and (I) with AS69- α S(N-B). Intensely fluorescent puncta corresponding to α S aggregates are indicated by white arrows. Nuclei were stained blue with Hoechst 33342. Scale bar in (C), 20 μ m (applies to all cell images).

schematized in Figure 8. Sequestration of αS monomers into the AS69: αS complex leads to the stoichiometric inhibition of fibril elongation. Upon formation of the 1:1 AS69: αS complex, substoichiometric inhibitory activity is gained that specifically targets fibril nucleation processes. For this inhibitory activity, two components are required. First, the globular part of the AS69: αS complex, including the region

Article





Intracellular inhibition of nucleation

Figure 8. Schematic overview of the inhibitory effect of the complex between AS69 and αS on amyloid formation

Figure360 ▷

For a Figure 360 author presentation of this figure, see https://doi.org/10.1016/j.xcrp.2024.102180. AS69 binds free α S monomer and inhibits elongation, whereas the complex between AS69 and α S inhibits nucleation processes. Shown on the bottom are the minimal fusion constructs that achieve substoichiometric inhibition of α S fibril nucleation and of aggregate seeding in biosensor cells.

 $\alpha S(30-60)$, is essential. This is demonstrated by the loss of inhibitory activity in αS fragments that are not fused to AS69. Second, the presence of αS IDRs is essential for substoichiometric inhibition. Interestingly, lipid-induced primary nucleation and secondary nucleation exhibit a difference in the required IDRs. While inhibition of secondary nucleation can be enabled by either the N terminus or the NAC region, inhibition of lipid-induced primary nucleation strictly necessitates the NAC region. The minimized active fusion constructs identified here are therefore AS69- $\alpha S(B-NAC)$ for primary nucleation and AS69- $\alpha S(B-NAC)$ or AS69- $\alpha S(N-B)$ for secondary nucleation, respectively (Figure 8).

The mechanism of inhibition of fibril elongation by monomer sequestration is easy to comprehend, considering that the α S-B region, which is an essential part of the α S fibril core, ^{28–31} is not available any longer for incorporation into the fibril structure upon binding to AS69. In line with this, AS69- α S, with pre-occupied α S binding site, does not inhibit fibril elongation (Figure 3).

In contrast, the substoichiometric activity of the AS69: α S complex on fibril nucleation is more challenging to elucidate. DGC of secondary nucleation assay samples detects low levels of oligomers from both α S and AS69- α S when fibril formation is



abrogated (Figures 4E-4G). α S and AS69- α S exhibit similar propensities to integrate into oligomers (Figure 4G), suggesting a scenario in which AS69-αS co-integrates with aS into pre-nucleus oligomers, whose further conversion into fibril nuclei is then hampered due to the presence of the AS69-bound α S-B region. This scenario is in line with the observation that the NAC IDR can enable the inhibition of both lipid-induced primary and secondary nucleation. The NAC region is the most hydrophobic segment of αS and critical for αS self-assembly. ^{32,33} The NAC IDR exposed on the AS69:αS complex might therefore drive the co-integration into αS pre-nucleus oligomers. The question arises: how does AS69-aS co-integrated into pre-nucleus oligomers prohibit their conversion into fibril nuclei? The AS69-bound aS-B region is critical for the substoichiometric inhibitory activity, as αS fragments without this region do not exhibit this activity (Figure 6). The AS69-bound α S-B region might act in different ways: (1) as in the case of elongation, it is not available any longer for incorporation into the fibril structure, which will prohibit the formation of a seedingcompetent fibril nucleus; (2) the globular complex of AS69 and αS-B represents a steric bulk that might interfere with the well-ordered assembly of other αS chains; (3) the globular complex of AS69 and α S-B might also more actively engage in a direct interaction with other parts of pre-nucleus oligomers; (4) AS69 binding to α S-B might alter the conformational ensembles of αS IDRs in subtle ways (i.e., with only minute resonance changes in ¹H-¹⁵N HSQC NMR spectroscopy [Figures 1C-1E], such as the modulation of transient long-range interactions). 34,35 Together, the AS69-bound α S-B region and the αS N and/or NAC IDRs achieve a remarkable substoichiometric activity, with one AS69-αS molecule being sufficient to achieve 50% suppression of secondary nucleation at a 50-fold excess of αS monomers (Figure 3C). This is striking when considering that the nucleus size will likely be much smaller than 50 α S units. A potential explanation would be a particularly high propensity of AS69- α S to partition into pre-nucleus oligomers (i.e., an enrichment of AS69-αS in pre-nucleus oligomers in comparison to α S). However, this is not supported by the DGC data, which indicate similar propensities of AS69- α S and α S for integration into oligomers. We therefore propose an alternative explanation: oligomers containing AS69-αS might not just be unable to convert into fibril nuclei themselves, but they might also gain an inherent activity to inhibit fibril nucleation. This activity, resulting in the substoichiometric inhibition of secondary nucleation, has been observed before for off-pathway oligomers in other amyloid systems and has been attributed to the blocking of secondary nucleation sites on the fibril surface by the oligomers.³⁶ Together, the inability of AS69-αS-containing oligomers to convert to fibril nuclei and an active role of these oligomers in the inhibition of secondary nucleation may explain the high efficiency of AS69- α S, particularly in inhibiting secondary nucleation.

For the inhibition of secondary nucleation, the NAC IDR is not required but it can be replaced by the N-terminal IDR (Figure 5C). This suggests that in secondary nucleation the αS N terminus can drive the incorporation into pre-nucleus oligomers. This is exactly the conclusion of recent NMR experiments that have found that αS monomers bind to αS fibrils via interactions of the monomers' N termini with C termini exposed on the fibril surface. The resulting dynamic alignment of N termini of fully unfolded αS molecules can trigger secondary nucleation. The αS N terminus also plays a role in lipid-induced primary nucleation, where it tethers the protein to the phospholipid membrane surface, leading to an increased local αS concentration that promotes aggregation. However, the inhibitory effect of AS69- αS (N-B) on secondary nucleation but not on lipid-induced primary nucleation suggests that the αS N terminus is more deeply involved in secondary nucleation, where it interacts with the unfolded αS C termini.

Article



Importantly, the activities of the different fusion constructs on amyloid formation in vitro correlate very well with their effects in cellular seeding assays. Thus, the αS IDRs that are important in the *in vitro* assays are also critical for the inhibition of seeding in biosensor cells (Figure 8). The precise mechanism of aggregate proliferation in biosensor cells has not been determined before. Here, we observed that cellular seeding is inhibited by all constructs that inhibit secondary nucleation *in vitro*. This strongly suggests that secondary nucleation drives aggregate seeding in αS biosensor cells. Thus, the monomers in seed-receiving cells do not only convert to the fibrillar state by addition to the fibril end template during fibril elongation, but they also form new fibril nuclei in secondary nucleation on the surface of added seeds.

The present study highlights the importance of IDR-IDR interactions in amyloid formation and its inhibition. Monomer binding agents are usually thought to affect protein assembly only at stoichiometric concentrations. Here, we observe that the complex of aggregation-prone monomers with monomer-binding agents can gain new inhibitory activity. In the case of AS69-αS, this activity depends on the presence of αS IDRs that remain unfolded in the AS69-bound state. As for the mechanistic basis, we find evidence that the IDRs can recruit the complex of inhibitor and amyloid protein monomers into oligomers formed by the latter, which block the conversion of oligomers into fibril nuclei. Furthermore, the inhibitor-containing oligomers might actively interfere with further nucleation processes. The processes underlying this inhibitory mechanism (complex formation, IDR presentation, oligomer formation, nucleation, inhibition of nucleation by incompatible oligomers) are generally applicable to amyloid proteins. Therefore, monomer-binding agents other than AS69, targeting αS , αS mutants, or other amyloid proteins, may act by the same mechanisms as AS69. For drug design, this strategy requires (1) targeting a binding site whose recruitment interferes with fibril nucleation (e.g., a segment indispensable for the formation of the cross-β fibril core) and (2) retaining sufficient IDRs in the amyloidogenic target upon drug-target complex formation to afford incorporation into oligomers. The particular capacity of IDRs to engage in variable interactions, which provides the basis for amyloid formation, can thus also be exploited to inhibit amyloid formation.

EXPERIMENTAL PROCEDURES

Elongation assay

Fibril elongation was monitored following established protocols. 19,39 Briefly, fibril seeds were produced in 20 mM 3-(N-morpholino)propanesulfonic acid (MOPS) (pH 7.4), 50 mM NaCl, in a 1.5-mL tube containing a glass bead at 37°C and 800 rpm for 75 h. Seeds were sonicated using a Hielscher UP200St ultrasonic processor for 30 s at 70% maximal amplitude. We prepared 100- μ L samples of 25 μ M α S monomers in 20 mM MOPS (pH 7.4), 50 mM NaCl, 20 μ M ThT, and 0.04% NaN3 in black 96-well half-area polystyrene plates with non-binding surface and clear bottom (ref. 3881, Corning), before adding sonicated seeds to a concentration of 2.5 μ M. Plates were sealed with clear sealing tape and placed into a FLUOstar Omega plate reader (BMG Labtech) for incubation at 37°C for 40 h. ThT was excited with a wavelength of 448 nm, and the emission was measured at 482 nm. Measurements were taken every 100 s in cycle 1–110 and every 300 s in a further 490 cycles.

Lipid-induced primary nucleation assay

Primary nucleation assays were performed in 50 mM NaPi (pH 6.5) in the presence of DMPS SUVs, as previously described. 9,13 Briefly, DMPS lipid powder was dissolved in 20 mM sodium phosphate (pH 6.5) and 0.01% NaN₃ and stirred at 45°C for 2 h. The



solutions were then frozen in dry ice and thawed at 45° C 5 times. Lipid vesicles were prepared by sonication using Bandelin Sonopuls MS72, 3 × 5 min, 50% cycle, 10% maximum power, and centrifuged at 15,000 rpm for 30 min at 25°C. We prepared 70- μ M α S monomers in 20 mM NaPi (pH 6.5), 50 mM NaCl, 20 μ M ThT, and 0.04% NaN₃ before adding 100 μ M DMPS SUVs. Measurements were performed as described for the elongation assay for 100 h, with measurements every 360 s for 1,000 cycles.

Secondary nucleation assay

Secondary nucleation assays were conducted as described, 13,19 with modifications outlined in Figure S5. Briefly, seed fibrils were produced in 20 mM acetate buffer (pH 5.0), 50 mM NaCl, in a 96-well plate along with a glass bead at 37°C and 500 rpm for at least 75 h. Seeds were sonicated using a Bandelin Sonopuls HD 2070 sonicator with MS-72 probe for 1 s at 10% maximal amplitude. We prepared 70- μ M α S monomers in 20 mM sodium acetate buffer (pH 5.0), 50 mM NaCl, 20 μ M ThT, and 0.04% NaN $_3$ before adding 0.3 μ M sonicated seeds. Measurements were performed as described for the elongation assay for 100 h, with measurements taken every 360 s for 1,000 cycles.

Density gradient ultracentrifugation

DGC was performed as previously described. 13,25 In short, 100- μ L samples were applied onto a discontinuous 25 mM sodium acetate, pH 5.0 buffered sucrose gradient layered in an 11- \times 34-mm centrifuge tube. The sucrose gradient contained the following volumes and concentration (w/w, from bottom to top): 300 μ L of 60%, 200 μ L of 50%, 200 μ L of 25%, 400 μ L of 20%, 400 μ L of 15%, 150 μ L of 10%, and 400 μ L of 5%. The gradients were centrifuged for 3 h at 259,000 \times g and 4°C in an Optima MAX-XP ultracentrifuge (Beckman Coulter) using a TLS-55 swing-out rotor (Beckman Coulter) and manually fractionated into 13 142- μ L fractions. The last fraction (14) was formed by the addition of 80 μ L 30 mM Tris-HCl, pH 7.4 buffer to the remaining volume.

Cell assay for aS aggregation

The pMK-RQ vector was used to carry a synthetic construct that encodes full-length A53T-mutated human aS fused with YFP at the C terminus (GeneArt, Thermo Fisher Scientific). The αSA53T-YFP construct was inserted into the pIRESpuro3 vector (Clontech, Takara Bio) via Nhel (5') and Notl (3') restriction sites. HEK293T cells (American Type Culture Collection) were cultured in high-glucose DMEM (Sigma-Aldrich) supplemented with 10% fetal calf serum (Sigma-Aldrich), 50 U/mL penicillin, and 50 μg/mL streptomycin (Sigma-Aldrich). The cells were cultured at 37°C in a humidified atmosphere containing 5% CO₂. Lipofectamine 2000 (Invitrogen, Thermo Fisher Scientific) was used to transfect the cells plated in DMEM. Stable cells were selected in DMEM containing 1 µg/mL puromycin (EMD Millipore). Monoclonal lines were generated by fluorescence-activated cell sorting of a polyclonal cell population in 96-well plates using a MoFlo XDP cell sorter (Beckman Coulter). Finally, the clonal cell line B5, referred to as αSA53T-YFP cells, was selected from among 24 clonal cell lines. The αSA53T-YFP cells were plated in a 384-well plate with poly-D-lysine coating (Greiner) at a density of 800 cells per well with 0.1 μ g/mL Hoechst 33342 (Thermo Fisher Scientific). To induce cellular aggregation of αS in $\alpha SA53T-YFP$ cells and to test its inhibition, fibrillar αS seeds (50 nM final concentration per well) were incubated with 1.5% Lipofectamine 2000 in Opti-MEM (Thermo Fisher Scientific) in the presence or absence of AS69-αS fusion constructs (15 μ M final concentration per well), for 2 h at room temperature. The resulting mixture was added to each well 4 h after the cells had been plated. The plate was incubated in a humidified atmosphere containing 5% CO₂ at 37°C. The cells were imaged using the blue and green fluorescence channels with an IN Cell Analyzer 6500HS System (Cytiva). The images were analyzed using IN Carta Image

Article



Analysis Software (Cytiva). To ensure objectivity, an automated algorithm was used to identify intracellular aggregates in living cells.

RESOURCE AVAILABILITY

Lead contact

Further information and requests for resources and reagents should be directed to and will be fulfilled by the lead contact, Wolfgang Hoyer (wolfgang.hoyer@hhu.de).

Materials availability

All unique/stable reagents generated in this study are available from the lead contact without restriction.

Data and code availability

Any additional information required to reanalyze the data reported in this paper is available from the lead contact upon request.

ACKNOWLEDGMENTS

This project received funding from the European Research Council under the European Union's Horizon 2020 research and innovation program, grant agreement no. 726368. We acknowledge Nina Kirchgässler for support with CD spectroscopy. We acknowledge access to the Jülich-Düsseldorf Biomolecular NMR Center.

AUTHOR CONTRIBUTIONS

C.M.S., G.T., and W.H. designed the experiments. C.M.S. and M.A. performed the experiments and analyzed the data. E.D.A. contributed analytical tools. L.G., H.H., and M.S. contributed to NMR data acquisition and analysis. C.M.S., G.T., and W.H. wrote the manuscript. All authors commented on the manuscript.

DECLARATION OF INTERESTS

The authors declare no competing interests.

SUPPLEMENTAL INFORMATION

Supplemental information can be found online at https://doi.org/10.1016/j.xcrp.2024.102180.

Received: March 25, 2024 Revised: July 7, 2024 Accepted: August 9, 2024 Published: September 2, 2024

REFERENCES

- Goedert, M., and Spillantini, M.G. (2012). Synucleinopathies and tauopathies. In Basic Neurochemistry (Elsevier), pp. 829–843. https://doi.org/10.1016/B978-0-12-374947-5. 00047-X.
- Spillantini, M.G., Crowther, R.A., Jakes, R., Hasegawa, M., and Goedert, M. (1998).
 α-Synuclein in filamentous inclusions of Lewy bodies from Parkinson's disease and dementia with Lewy bodies. Proc. Natl. Acad. Sci. USA 95, 6469–6473. https://doi.org/10.1073/pnas. 95.11.6469.
- Knowles, T.P.J., Vendruscolo, M., and Dobson, C.M. (2014). The amyloid state and its association with protein misfolding diseases. Nat. Rev. Mol. Cell Biol. 15, 384–396. https:// doi.org/10.1038/nrm3810.
- 4. Meisl, G., Kirkegaard, J.B., Arosio, P., Michaels, T.C.T., Vendruscolo, M., Dobson, C.M., Linse, S., and Knowles, T.P.J. (2016). Molecular

- mechanisms of protein aggregation from global fitting of kinetic models. Nat. Protoc. 11, 252–272. https://doi.org/10.1038/nprot. 2016.010.
- Iadanza, M.G., Jackson, M.P., Hewitt, E.W., Ranson, N.A., and Radford, S.E. (2018). A new era for understanding amyloid structures and disease. Nat. Rev. Mol. Cell Biol. 19, 755–773. https://doi.org/10.1038/ s41580-018-0060-8.
- Chatani, E., and Yamamoto, N. (2018). Recent progress on understanding the mechanisms of amyloid nucleation. Biophys. Rev. 10, 527–534. https://doi.org/10.1007/s12551-017-0353-8.
- Xue, W.F., Homans, S.W., and Radford, S.E. (2008). Systematic analysis of nucleationdependent polymerization reveals new insights into the mechanism of amyloid selfassembly. Proc. Natl. Acad. Sci. USA 105, 8926–

- 8931. https://doi.org/10.1073/pnas. 0711664105.
- Arosio, P., Knowles, T.P.J., and Linse, S. (2015).
 On the lag phase in amyloid fibril formation.
 Phys. Chem. Chem. Phys. 17, 7606–7618.
 https://doi.org/10.1039/c4cp05563b.
- Galvagnion, C., Buell, A.K., Meisl, G., Michaels, T.C.T., Vendruscolo, M., Knowles, T.P.J., and Dobson, C.M. (2015). Lipid vesicles trigger α-synuclein aggregation by stimulating primary nucleation. Nat. Chem. Biol. 11, 229–234. https://doi.org/10.1038/ nchembio.1750.
- Viennet, T., Wördehoff, M.M., Uluca, B., Poojari, C., Shaykhalishahi, H., Willbold, D., Strodel, B., Heise, H., Buell, A.K., Hoyer, W., and Etzkorn, M. (2018). Structural insights from lipid-bilayer nanodiscs link α-synuclein membrane-binding modes to amyloid fibril



Cell Reports Physical Science Article

- formation. Commun. Biol. 1, 44. https://doi.org/10.1038/s42003-018-0049-z.
- 11. Linse, S. (2017). Monomer-dependent secondary nucleation in amyloid formation. Biophys. Rev. 9, 329–338. https://doi.org/10.1007/s12551-017-0289-z.
- Young, L.M., Ashcroft, A.E., and Radford, S.E. (2017). Small molecule probes of protein aggregation. Curr. Opin. Chem. Biol. 39, 90–99. https://doi.org/10.1016/j.cbpa.2017. 06.008
- Agerschou, E.D., Flagmeier, P., Saridaki, T., Galvagnion, C., Komnig, D., Heid, L., Prasad, V., Shaykhalishahi, H., Willbold, D., Dobson, C.M., et al. (2019). An engineered monomer binding-protein for α-synuclein efficiently inhibits the proliferation of amyloid fibrils. Elife 8, e46112. https://doi.org/10.7554/elife.46112.
- Mirecka, E.A., Shaykhalishahi, H., Gauhar, A., Akgül, Ş., Lecher, J., Willbold, D., Stoldt, M., and Hoyer, W. (2014). Sequestration of a β-Hairpin for Control of α-Synuclein Aggregation. Angew. Chem. Int. Ed. 53, 4227– 4230. https://doi.org/10.1002/anie.201309001.
- Liang, Z., Chan, H.Y.E., Lee, M.M., and Chan, M.K. (2021). A SUMO1-Derived Peptide Targeting SUMO-Interacting Motif Inhibits α-Synuclein Aggregation. Cell Chem. Biol. 28, 180–190.e6. https://doi.org/10.1016/j. chembiol.2020.12.010.
- Ahmed, J., Fitch, T.C., Donnelly, C.M., Joseph, J.A., Ball, T.D., Bassil, M.M., Son, A., Zhang, C., Ledreux, A., Horowitz, S., et al. (2022). Foldamers reveal and validate therapeutic targets associated with toxic α-synuclein selfassembly. Nat. Commun. 13, 2273. https://doi. org/10.1038/s41467-022-29724-4.
- Burmann, B.M., Gerez, J.A., Matečko-Burmann, I., Campioni, S., Kumari, P., Ghosh, D., Mazur, A., Aspholm, E.E., Šulskis, D., Wawrzyniuk, M., et al. (2020). Regulation of α-synuclein by chaperones in mammalian cells. Nature 577, 127–132. https://doi.org/10.1038/ s41586-019-1808-9.
- Gauhar, A., Shaykhalishahi, H., Gremer, L., Mirecka, E.A., and Hoyer, W. (2014). Impact of subunit linkages in an engineered homodimeric binding protein to α-synuclein. Protein Eng. Des. Sel. 27, 473–479. https://doi. org/10.1093/protein/gzu047.
- Buell, A.K., Galvagnion, C., Gaspar, R., Sparr, E., Vendruscolo, M., Knowles, T.P.J., Linse, S., and Dobson, C.M. (2014). Solution conditions determine the relative importance of nucleation and growth processes in α-synuclein aggregation. Proc. Natl. Acad. Sci. USA 111, 7671–7676. https://doi.org/10.1073/pnas. 1315346111.
- 20. Flagmeier, P., Meisl, G., Vendruscolo, M., Knowles, T.P.J., Dobson, C.M., Buell, A.K., and Galvagnion, C. (2016). Mutations associated

- with familial Parkinson's disease alter the initiation and amplification steps of α -synuclein aggregation. Proc. Natl. Acad. Sci. USA 113, 10328–10333. https://doi.org/10.1073/pnas. 1604645113.
- Xue, W.-F., Hellewell, A.L., Gosal, W.S., Homans, S.W., Hewitt, E.W., and Radford, S.E. (2009). Fibril fragmentation enhances amyloid cytotoxicity. J. Biol. Chem. 284, 34272–34282. https://doi.org/10.1074/jbc.M109.049809.
- Campioni, S., Carret, G., Jordens, S., Nicoud, L., Mezzenga, R., and Riek, R. (2014). The presence of an air–water interface affects formation and elongation of α-synuclein fibrils. J. Am. Chem. Soc. 136, 2866–2875. https://doi. org/10.1021/ja412105t.
- 23. LeVine, H. (1995). Thioflavine T interaction with amyloid β-sheet structures. Amyloid 2, 1–6. https://doi.org/10.3109/13506129509031881.
- Xue, C., Lin, T.Y., Chang, D., and Guo, Z. (2017). Thioflavin T as an amyloid dye: fibril quantification, optimal concentration and effect on aggregation. R. Soc. Open Sci. 4, 160696. https://doi.org/10.1098/rsos.160696.
- Rösener, N.S., Gremer, L., Wördehoff, M.M., Kupreichyk, T., Etzkorn, M., Neudecker, P., and Hoyer, W. (2020). Clustering of human prion protein and a-synuclein oligomers requires the prion protein N-terminus. Commun. Biol. 3, 365. https://doi.org/10.1038/s42003-020-1085-z.
- Arosio, P., Vendruscolo, M., Dobson, C.M., and Knowles, T.P.J. (2014). Chemical kinetics for drug discovery to combat protein aggregation diseases. Trends Pharmacol. Sci. 35, 127–135. https://doi.org/10.1016/j.tips.2013.12.005.
- Xu, Y., Maya-Martinez, R., and Radford, S.E. (2022). Controlling amyloid formation of intrinsically disordered proteins and peptides: slowing down or speeding up? Essays Biochem. 66, 959–975. https://doi.org/10. 1042/ebc20220046.
- Agerschou, E.D., Schützmann, M.P., Reppert, N., Wördehoff, M.M., Shaykhalishahi, H., Buell, A.K., and Hoyer, W. (2021). β-Turn exchanges in the α-synuclein segment 44-TKEG-47 reveal high sequence fidelity requirements of amyloid fibril elongation. Biophys. Chem. 269, 106519. https://doi.org/10.1016/j.bpc.2020.106519.
- Guerrero-Ferreira, R., Taylor, N.M., Arteni, A.A., Kumari, P., Mona, D., Ringler, P., Britschgi, M., Lauer, M.E., Makky, A., Verasdonck, J., et al. (2019). Two new polymorphic structures of human full-length α-synuclein fibrils solved by cryo-electron microscopy. Elife 8, e48907. https://doi.org/10. 7554/eLife.48907.
- Li, B., Ge, P., Murray, K.A., Sheth, P., Zhang, M., Nair, G., Sawaya, M.R., Shin, W.S., Boyer, D.R., Ye, S., et al. (2018). Cryo-EM of full-length α-synuclein reveals fibril polymorphs with a

- common structural kernel. Nat. Commun. 9, 3609. https://doi.org/10.1038/s41467-018-05971-2.
- Li, Y., Zhao, C., Luo, F., Liu, Z., Gui, X., Luo, Z., Zhang, X., Li, D., Liu, C., and Li, X. (2018). Amyloid fibril structure of α-synuclein determined by cryo-electron microscopy. Cell Res. 28, 897–903. https://doi.org/10.1038/ s41422-018-0075-x.
- Giasson, B.I., Murray, I.V., Trojanowski, J.Q., and Lee, V.M. (2001). A hydrophobic stretch of 12 amino acid residues in the middle of α-synuclein is essential for filament assembly.
 J. Biol. Chem. 276, 2380–2386. https://doi.org/ 10.1074/jbc.m008919200.
- Zibaee, S., Fraser, G., Jakes, R., Owen, D., Serpell, L.C., Crowther, R.A., and Goedert, M. (2010). Human β-synuclein rendered fibrillogenic by designed mutations. J. Biol. Chem. 285, 38555–38567. https://doi.org/10. 1074/jbc.m110.160721.
- Esteban-Martín, S., Silvestre-Ryan, J., Bertoncini, C.W., and Salvatella, X. (2013). Identification of fibril-like tertiary contacts in soluble monomeric α-synuclein. Biophys. J. 105, 1192–1198. https://doi.org/10.1016/j.bpj. 2013.07.044.
- Bertoncini, C.W., Jung, Y.-S., Fernandez, C.O., Hoyer, W., Griesinger, C., Jovin, T.M., and Zweckstetter, M. (2005). Release of long-range tertiary interactions potentiates aggregation of natively unstructured α-synuclein. Proc. Natl. Acad. Sci. USA 102, 1430–1435. https://doi. org/10.1073/pnas.0407146102.
- Hasecke, F., Niyangoda, C., Borjas, G., Pan, J., Matthews, G., Muschol, M., and Hoyer, W. (2021). Protofibril-Fibril Interactions Inhibit Amyloid Fibril Assembly by Obstructing Secondary Nucleation. Angew. Chem. Int. Ed. 60, 3016–3021. https://doi.org/10.1002/anie. 202010098.
- Yang, X., Wang, B., Hoop, C.L., Williams, J.K., and Baum, J. (2021). NMR unveils an N-terminal interaction interface on acetylated-α-synuclein monomers for recruitment to fibrils. Proc. Natl. Acad. Sci. USA 118, e2017452118. https://doi. org/10.1073/pnas.2017452118.
- Kumari, P., Ghosh, D., Vanas, A., Fleischmann, Y., Wiegand, T., Jeschke, G., Riek, R., and Eichmann, C. (2021). Structural insights into α-synuclein monomer–fibril interactions. Proc. Natl. Acad. Sci. USA 118, e2012171118. https:// doi.org/10.1073/pnas.2012171118.
- Agerschou, E.D., Borgmann, V., Wördehoff, M.M., and Hoyer, W. (2020). Inhibitor and substrate cooperate to inhibit amyloid fibril elongation of α-synuclein. Chem. Sci. 11, 11331–11337. https://doi.org/10.1039/ D05C04051G.